

# Terrain Vision Aided Online Estimation of Instantaneous Centers of Rotation for Skid-Steering Mobile Robots\*

Wenjun Lv<sup>1</sup>, Ji Chang<sup>1</sup>, Yu Kang<sup>2</sup>, Yun-Bo Zhao<sup>3</sup>, and Zerui Li<sup>1</sup>

**Abstract**—Skid-steering mobile robots suffer from slip effect inevitably during their turnings, which results in imprecise kinematics model and the degradation of navigation and control performances. Hence, in this paper, we aim at developing an online estimation method to acquire the robot's instantaneous centers of rotation (ICRs), a kind of slip parameters, by means of data fusion technologies. The sensor system is composed of two incremental encoders, a compass, a Global Positioning System (GPS) unit, a camera and a data fusion unit. Based on the data gathered from these sensors, the data fusion unit is able to provide accurate global location, absolute heading and robot's ICRs in real time by applying the proposed terrain adaptive innovation-based extended Kalman filter. With the aid of terrain vision, the process noise covariance can be adjusted according to the terrain type adaptively, and therefore, the ICR estimation converges rapidly and smoothly. The real-world experiment conducted on a four-wheel mobile robot is exhibited to validate the effectiveness. Additionally, the results show that the terrain adaptive odometry has higher accuracy than the traditional ones.

## I. INTRODUCTION

Skid-steering mobile robots are able to govern their headings by adjusting the relative speed between the left and right wheels rather than resorting to independent steering mechanisms. Due to its robustness, simplicity and ability of zero-radius turn, skid-steering mobile robots have become the preferred all-terrain robots in agriculture, industry and military. For the presence of large contacting patch between wheels and terrains, the unpredicted slip is inevitable which makes it difficult to build a precise kinematics model [1]. However, because most strategies concerning navigation, motion control, obstacle avoidance and route planning are designed based on the kinematics model of skid-steering mobile robot, the robot's performance can be significantly improved by the online identification of terrain-related slip parameters which are included in the kinematics model [2]–[7]. Therefore, in this paper, we concentrate on designing a

data fusion approach to acquire slip parameters in real time.

For the fact that the instantaneous centres of rotation (ICRs) of the robot's chassis, wheels or tracks are almost constant while the mobile robot is moving on the same terrain, the ICR kinematics model was proposed by introducing the ICRs into the traditional kinematics model of skid-steering mobile robot [8]. The positions the ICRs is able to reflect the robot's lateral and longitude slips on different terrains, so they can be read as the slip parameters, and therefore, we are in the position to develop an ICR estimation method. In [9], an empirical model combining ICRs and robot's kinematics state (i.e., the forward speed and radius of the path curvature) is experimentally established, which has proven to significantly improve the performance of dead reckoning. The primary issue of such an off-line method is that the robot-terrain mapping database should be established in advance, so the ICR estimation can not proceed when the mobile robot enters the area where the terrain is not included in this database. Therefore, the current attentions are switched to develop on-line ICR estimation methods. Because the states of an ICR kinematics model is composed of the robot's pose and ICRs, we can estimate the ICRs by fusing an odometry, heading sensor, and positioning system. This work has been done by employing an extended Kalman filter (EKF), and its effectiveness has been verified by a number of experiments when the mobile robot traverses the terrains in different motion patterns [10].

However, due to the uncertainties in the ICR kinematics model and the linearization-induced error during the procedure of EKF, the EKF-based ICR estimation method may lose accuracy or even become unreliable. Furthermore, the sudden terrain change and kinematics states' variation may result in the degradation of system performance as well. In [11], a strong tracking filter (STF) and standard Kalman filter are applied to estimate the robot's kinematics states and ICRs, respectively. By introducing a suboptimal fading scaling factors, the filtering gain can be adjusted to guarantee the orthogonality of innovation series. Hence, this method has better state tracking ability and higher robustness against model uncertainties and state jump.

To the best of our knowledge, the aforementioned work is the state-of-the-art technologies concerning the ICR estimation. The existing studies focus on the fusion approach, such as the Kalman filter and its extensions, which suffer from the following two common issues. First, the process noise covariance of ICRs should be set as a relatively large constant to enable the rapid convergence of ICR estimation, but the ICR estimation results will oscillate seriously around the

\*This work was supported in part by the National Natural Science Foundation of China (61725304 and 61673361). Authors also gratefully acknowledge supports from the Youth Top-notch Talent Support Program, the 1000-talent Youth Program and the Youth Yangtze River Scholar.

<sup>1</sup>Wenjun Lv, Ji Chang and Zerui Li are with the Department of Automation, University of Science and Technology of China, Hefei 230027, China. lvwenjun@mail.ustc.edu.cn

<sup>2</sup>Yu Kang, the corresponding author, is with the State Key Laboratory of Fire Science, Department of Automation and Institute of Advanced Technology, University of Science and Technology of China, Hefei 230027, China. He is also with the Key Laboratory of Technology in GeoSpatial Information Processing and Application System, Chinese Academy of Sciences, Beijing 100190, China. kangduyu@ustc.edu.cn

<sup>3</sup>Yun-bo Zhao is with the College of Information Engineering, Zhejiang University of Technology, Hangzhou 310023, China. ybzhao@zjut.edu.cn

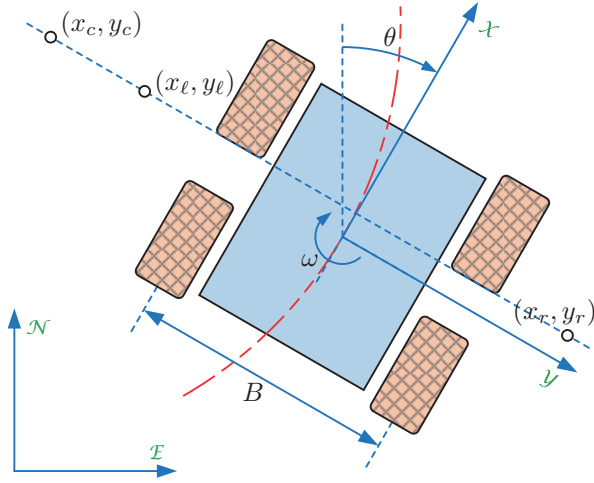


Fig. 1: Top-view schematic of a skid-steering robot on a planar floor. The two yellow meshed rectangles represent robot wheels and the blue rectangle represents robot chassis.

truth values. On the contrary, to guarantee the smoothness, the process noise covariance should be set as a relatively small constant at the cost of slow convergence. Hence, the setup of process noise covariance faces a inevitable trade-off between the convergence rate and the smoothness of ICR estimation. Second, the bad weather, canopy and viaduct may block the satellite signals to some extent, resulting in a lower localization accuracy of GPS. The ferrous and electric materials may degrade the compass performance as well. Hence, the time-varying statistical characteristics of observations should be taken into consideration. In order to solve the two issues, we propose a terrain adaptive innovation based extended Kalman filter (terrain adaptive IEKF), to fuse the data gathered from the incremental encoders, compass, GPS unit and camera.

The rest of the paper is organized as follows. Section II covers the establishment of the ICR kinematics model. Section III presents the details of the proposed terrain adaptive innovation based extended Kalman filter. Section IV exhibits a real-world experiment and its result analysis. In Section V, the paper is concluded.

## II. ICR KINEMATICS MODEL

This chapter expatiates the kinematics model of skid-steering robot by introducing the instantaneous centres of rotation (ICRs) which are illustrated in Fig. 1. The body coordinate system (BCS) is assumed to have its origin on the geometric centre of robot chassis. The  $X$ -axis and  $Y$ -axis are aligned with the longitudinal forward direction and lateral rightward direction, respectively. The  $E$ -axis and  $N$ -axis of world coordinate system (WCS) are eastward and northward, respectively.

For a skid-steering robot, the following assumptions are taken into consideration.

- All the wheels on the same side have the same rotational speed.
- All wheels are in contact with the ground.

- The moving plane is planar.
- All wheels are same in size and their radii are time-invariant.

The kinematics states with respect to BCS and WCS can be related by

$$\begin{bmatrix} \dot{e} \\ \dot{n} \\ \dot{\theta} \end{bmatrix} = \begin{bmatrix} \sin \theta & \cos \theta & 0 \\ \cos \theta & -\sin \theta & 0 \\ 0 & 0 & 1 \end{bmatrix} \begin{bmatrix} v_x \\ v_y \\ \omega \end{bmatrix}, \quad (1)$$

where  $e$  and  $n$  denote the eastward and northward location coordinate with respect to WCS,  $\theta$  denotes the robot heading angle with respect to WCS,  $\omega$  denotes the rolling speed and  $v_x$  and  $v_y$  denote the translational speeds parallel to the  $X$ -axis and  $Y$ -axis,

Now we are in the position to find the relationship between  $v_x$ ,  $v_y$ ,  $\omega$  and wheel rotational speeds by introducing ICRs. Regarding the robot chassis, the left-side wheels and the right-side wheels as three rigid bodies, their ICRs can be described as three points with respect to BCS as shown in Fig. 1. The three ICRs locates on the same line parallel to the  $X$ -axis. Geometrically, the coordinates  $(x_c, y_c)$ ,  $(x_l, y_l)$ ,  $(x_r, y_r)$  are functions of the rolling and translational speeds, that is [8]

$$x_c = x_l = x_r = -\frac{v_y}{\omega}, \quad (2a)$$

$$y_l = \frac{v_x - v_l}{\omega}, \quad (2b)$$

$$y_r = \frac{v_x - v_r}{\omega}, \quad (2c)$$

$$y_c = \frac{v_x}{\omega}, \quad (2d)$$

where  $v_l$  and  $v_r$  denote the rotational speeds of the left-side and right-side wheels. The value of  $x_c$  could be any real number within  $(-\infty, +\infty)$  theoretically and the infinities are reached when  $\omega = 0$ . However, the values of  $y_c$ ,  $x_l$  and  $x_r$  are bounded because the numerators and denominators of (2a), (2b) and (2c) are infinitesimals of the same order while the robot is in linear motion.

Furthermore, the instantaneous rolling and translational speeds with respect to BCS can be obtained by computing the inverse function of (2a), (2b), (2c) and (2d), that is

$$v_x = \frac{v_r y_l - v_l y_r}{y_l - y_r}, \quad (3a)$$

$$v_y = \frac{x_c(v_l - v_r)}{y_l - y_r}, \quad (3b)$$

$$\omega = \frac{v_r - v_l}{y_l - y_r}. \quad (3c)$$

It can be known from (3a), (3b) and (3c) that the precise kinematics model of skid-steering robot can be obtained if  $x_l$ ,  $x_r$  and  $y_c$  are known. All the slip effects caused by, for example, the imbalance tire-ground contact forces and asymmetric mass distributions, can be reflected by the three parameters.

$$\begin{bmatrix} e_{t+1} \\ n_{t+1} \\ \theta_{t+1} \\ y_{\ell,t+1} \\ y_{r,t+1} \\ x_{c,t+1} \end{bmatrix} = \begin{bmatrix} e_t + T \left( \frac{v_{r,t}y_{\ell,t} - v_{\ell,t}y_{r,t}}{y_{\ell,t} - y_{r,t}} \sin \theta_t + \frac{x_{c,t}(v_{\ell,t} - v_{r,t})}{y_{\ell,t} - y_{r,t}} \cos \theta_t \right) \\ n_t + T \left( \frac{v_{r,t}y_{\ell,t} - v_{\ell,t}y_{r,t}}{y_{\ell,t} - y_{r,t}} \cos \theta_t - \frac{x_{c,t}(v_{\ell,t} - v_{r,t})}{y_{\ell,t} - y_{r,t}} \sin \theta_t \right) \\ \theta_t + T \left( \frac{v_{r,t} - v_{\ell,t}}{y_{\ell,t} - y_{r,t}} \right) \\ y_{\ell,t} \\ y_{r,t} \\ x_{c,t} \end{bmatrix} + T \cdot \begin{bmatrix} w_{e,t} \\ w_{n,t} \\ w_{\theta,t} \\ w_{\ell,t} \\ w_{r,t} \\ w_{c,t} \end{bmatrix} \quad (5)$$

$$F_{\mathcal{K},t} = \begin{bmatrix} 1 & 0 & T \left( \frac{v_{r,t}\hat{y}_{\ell,t} - v_{\ell,t}\hat{y}_{r,t}}{\hat{y}_{\ell,t} - \hat{y}_{r,t}} \cos \hat{\theta}_t + \frac{\hat{x}_{c,t}(v_{r,t} - v_{\ell,t})}{\hat{y}_{\ell,t} - \hat{y}_{r,t}} \sin \hat{\theta}_t \right) \\ 0 & 1 & T \left( \frac{v_{\ell,t}\hat{y}_{r,t} - v_{r,t}\hat{y}_{\ell,t}}{\hat{y}_{\ell,t} - \hat{y}_{r,t}} \sin \hat{\theta}_t + \frac{\hat{x}_{c,t}(v_{r,t} - v_{\ell,t})}{\hat{y}_{\ell,t} - \hat{y}_{r,t}} \cos \hat{\theta}_t \right) \\ 0 & 0 & 1 \end{bmatrix} \quad (6a)$$

$$F_{\mathcal{S},t} = T(v_{\ell,t} - v_{r,t}) \begin{bmatrix} \frac{\hat{y}_{r,t} \sin \hat{\theta}_t}{(\hat{y}_{\ell,t} - \hat{y}_{r,t})^2} - \frac{\hat{x}_{c,t} \cos \hat{\theta}_t}{(\hat{y}_{\ell,t} - \hat{y}_{r,t})^2} & \frac{-\hat{y}_{\ell,t} \sin \hat{\theta}_t}{(\hat{y}_{\ell,t} - \hat{y}_{r,t})^2} + \frac{\hat{x}_{c,t} \cos \hat{\theta}_t}{(\hat{y}_{\ell,t} - \hat{y}_{r,t})^2} & \frac{\cos \hat{\theta}_t}{\hat{y}_{\ell,t} - \hat{y}_{r,t}} \\ \frac{\hat{y}_{r,t} \cos \hat{\theta}_t}{(\hat{y}_{\ell,t} - \hat{y}_{r,t})^2} + \frac{\hat{x}_{c,t} \sin \hat{\theta}_t}{(\hat{y}_{\ell,t} - \hat{y}_{r,t})^2} & \frac{-\hat{y}_{\ell,t} \cos \hat{\theta}_t}{(\hat{y}_{\ell,t} - \hat{y}_{r,t})^2} - \frac{\hat{x}_{c,t} \sin \hat{\theta}_t}{(\hat{y}_{\ell,t} - \hat{y}_{r,t})^2} & \frac{-\sin \hat{\theta}_t}{\hat{y}_{\ell,t} - \hat{y}_{r,t}} \\ \frac{-1}{(\hat{y}_{\ell,t} - \hat{y}_{r,t})^2} & \frac{1}{(\hat{y}_{\ell,t} - \hat{y}_{r,t})^2} & 0 \end{bmatrix} \quad (6b)$$

### III. TERRAIN ADAPTIVE IEKF

To facilitate the implementation of state estimation in digital devices, we derive the discrete-time form of ICR kinematics model as

$$s_{t+1} = f(s_t, v_{\ell,t}, v_{r,t}) + w_t, \quad (4)$$

where  $s_t = [e_t, n_t, \theta_t, y_{\ell,t}, y_{r,t}, x_{c,t}]'$  denotes the state vector, and  $w_t = [w_{e,t}, w_{n,t}, w_{\theta,t}, w_{\ell,t}, w_{r,t}, w_{c,t}]'$  denotes the process noise vector which is assumed as Gaussian white noises. Combining all the equations appeared in Section II, the specific form of (4) can be obtained as shown in (5) after using Euler method.

The previous work has shown that the ICR locations are approximately constant while the robot is moving on a hard and flat ground regardless of its manoeuvring patterns [8]. Hence, the ICR locations can be modelled as a Markov-Gaussian stochastic process, that is, the ICR locations at the current sampling point equals the sum of those at the last sampling point and additive Gaussian white noises.

The observation equation follows the following form

$$z_t = Hs_t + v_t, \quad (7)$$

where  $z_t = [z_{e,t}, z_{n,t}, z_{\theta,t}]'$  denotes the observation vector,  $v_t = [v_{e,t}, v_{n,t}, v_{\theta,t}]'$  denotes the observation noise vector

which is assumed as Gaussian white noises, and  $H = [I_{3 \times 3}, O_{3 \times 3}]$  denotes the observation matrix where  $O_{3 \times 3}$  and  $I_{3 \times 3}$  denotes a  $3 \times 3$  null matrix and identity matrix respectively.

Now we are in the position to realize the ICR estimation by fusing (4) and (7). There are two issues should be taken into consideration: 1) The observation noise variance  $R$  may varying with the robot motion, e. g., the performances of GPS and compass degrade when the mobile robot moves into the areas with a lot of buildings or magnetic interference. Hence, the accuracy of EKF-based ICR estimation decreases; 2) If the process noise variances of ICRs are set as three relatively small constants, the results of ICR estimation will be smooth, but the convergence is slow when terrain changes. On the contrary, if the process noise variances of ICRs are set as three relatively large constants, the ICR estimation results will oscillate seriously around the truth values. Hence, the setup of process noise variances faces a inevitable trade-off between the convergence rate and smoothness of the ICR estimation.

Therefore, we propose the terrain adaptive innovation based extended Kalman filter (terrain adaptive IEKF) to solve such a data fusion problem. The IEKF is an adaptive filtering algorithm which introduces a innovation covariance

estimator into the calculation of the Kalman gain, thus to be robust against varying noise statistical characteristics, model uncertainties or linearization-induced error [12]. The details of terrain adaptive IEKF are shown as follows.

1) *Predicted Estimation*: The predicted estimation  $\tilde{s}_t$  is

$$\tilde{s}_{t+1} = f(\hat{s}_t, v_{\ell,t}, v_{r,t}), \quad (8)$$

where  $f(\cdot)$  has the form shown in (5). The error variance of  $\tilde{s}_{t+1}$  is

$$\tilde{P}_{t+1} = F_t \hat{P}_t F_t' + L_t Q L_t', \quad (9)$$

where  $F_t$  and  $L_t$  denote the Jacobian matrices of  $f(\cdot)$ , that is,

$$F_t = \left. \frac{\partial f}{\partial s_t} \right|_{s_t = \hat{s}_t} = \begin{bmatrix} F_{\mathcal{K},t} & F_{S,t} \\ O_{3 \times 3} & I_{3 \times 3} \end{bmatrix}, \quad (10a)$$

$$L_t = \left. \frac{\partial f}{\partial w_t} \right|_{s_t = \hat{s}_t} = T \cdot I_{6 \times 6}, \quad (10b)$$

where  $O_{n \times n}$  and  $I_{n \times n}$  denotes  $n \times n$  null matrix and identity matrix respectively. The specific forms of  $F_{\mathcal{K},t}$  and  $F_{S,t}$  are shown in (6a) and (6b), respectively. The process noise variance  $Q = \text{diag}(q_1, q_2, q_3, q_4, q_5, q_6)$  is a diagonal matrix. The process noise variance of ICRs  $\bar{Q} = \text{diag}(q_4, q_5, q_6)$  is set as  $\bar{Q}_{\min} = \text{diag}(q_{\min}, q_{\min}, q_{\min})$  where  $q_{\min}$  is a relatively small positive number, say 0.01.

2) *Terrain Visual Adjustment*: The feature vector of a terrain image at sampling point  $t$  is denoted by  $c_t = [c_{r,t}, c_{g,t}, c_{b,t}, c_{\ell,t}]'$ , where  $c_r$ ,  $c_g$  and  $c_b$  denotes three  $D$ -dimensional vectors which are related to three  $D$ -divided color histograms with respect to the RGB colour space,  $c_{\ell}$  also denotes a  $D$ -dimensional vector representing the image textures. After graying the original coloured image, we use Local Binary Pattern (LBP) to acquire the LBP feature diagram with  $D$  resolutions, thus obtaining  $c_{\ell}$ . Hence,  $c_t$  is a  $4D$ -dimensional vector.

Define a similarity function  $\phi_t = \|c_t - c_{t-1}\|$  where  $\|\cdot\|$  denotes the  $\ell_2$ -norm. If  $\phi_t > \sigma$  where  $\sigma$  is a positive number, then  $\bar{Q}$  is set as  $\bar{Q}_{\max} = \text{diag}(q_{\max}, q_{\max}, q_{\max})$  where  $q_{\max}$  is a relatively large positive number, say 100. After 5 sampling points,  $\bar{Q}$  is restored to  $\bar{Q}_{\min}$ .

3) *Corrected Estimation*: The innovation  $\delta_{t+1}$  is

$$\delta_{t+1} = z_{t+1} - H\tilde{s}_{t+1}, \quad (11)$$

and its covariance can be estimated by

$$\begin{aligned} \Delta_{t+1} &= \frac{1}{N} \sum_{i=t-N+2}^{t+1} \delta_i \delta_i' \\ &= \Delta_t + \frac{1}{N} (\delta_{t+1} \delta_{t+1}' - \delta_{t-N+2} \delta_{t-N+2}'), \end{aligned} \quad (12)$$

where  $N$  denotes the window size. Furthermore, the filtering gain  $K_t$  is obtained,

$$K_{t+1} = \tilde{P}_{t+1} H' \Delta_{t+1}^{-1}. \quad (13)$$

Finally, the corrected estimation  $\hat{s}_{t+1}$  is

$$\hat{s}_{t+1} = \tilde{s}_{t+1} + K_{t+1} \delta_{t+1}, \quad (14)$$

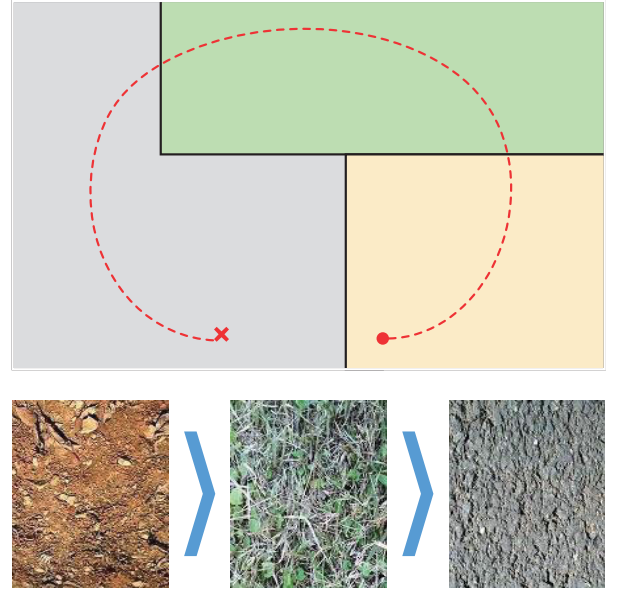


Fig. 2: Illustrations of experiment scenarios. The yellow, green and gray areas represent the terrains of soil, grass and asphalt, respectively. The red disc, cross and dashed curve represent the origin, destination and planned route, respectively.

coupled with its error variance

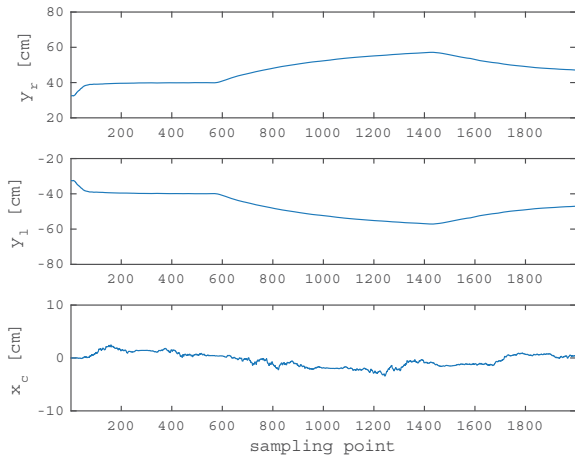
$$\hat{P}_{t+1} = (I_{6 \times 6} - K_{t+1} H) \tilde{P}_{t+1}. \quad (15)$$

#### IV. EXPERIMENTAL VERIFICATION

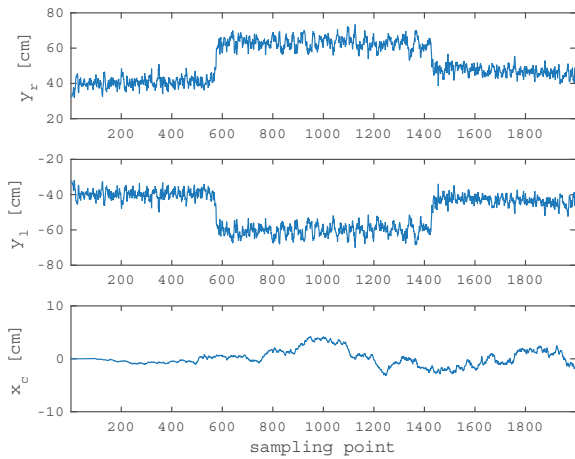
In this section, a real-world experiment based on a four-wheeled mobile robot, equipping with two incremental encoders, a GPS-compass integrated unit, and a downward-looking camera, is presented to verify the effectiveness of the proposed terrain adaptive IEKF. We mainly focus on the convergence rate and smoothness of the ICR estimation. Additionally, it is demonstrated that the accuracy of dead reckoning could be improved with the knowledge of ICRs.

The experimental mobile robot is 400 millimeters in length, 320 millimeters in width, and 250 millimeters in height. The four wheels share the same diameter (130 millimeters) and width (60 millimeters). One of the left-side wheels is equipped with a incremental encoder of 540 resolutions, as well as the right-side wheels. The GPS-compass integrated unit is able to output the robot's pose (including the position and orientation) at 1 Hz with accuracies of 2 meters and 1 degrees. The camera captures the terrain images of  $640 \times 480$  resolutions every ten seconds. As shown in Fig. 2, during the experiment, the mobile robot traversed the soil, grass and asphalt terrains, successively, and gathered the data from the sensors at the rate of 1 Hz. After the data gathering, these data are send to a computer (3.2 GHz with 8 GB RAM), and processed by using MATLAB.

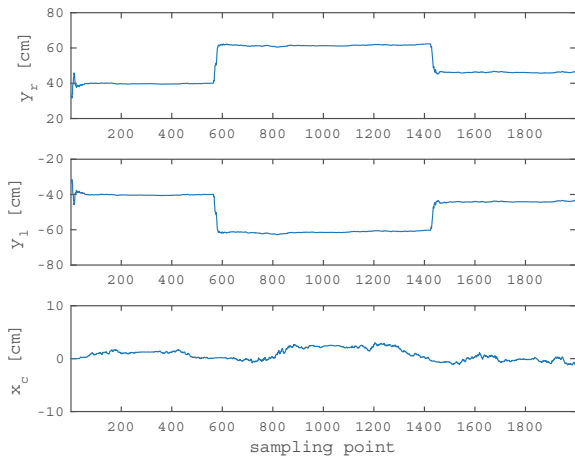
In Test 1 where  $q_{\min} = 0.1^2$ , as shown in Fig. 3a, the convergent tendency is obvious, but it takes too much time to track the truths of ICRs. If the terrain changes frequently,



(a) Results for Test 1.



(b) Results for Test 2.



(c) Results for Test 3.

Fig. 3: Results of ICR estimation test.

the ICR estimation may not track the truths. The results of Test 2 where  $q_{\max} = 20^2$  are shown in Fig. 3b. The ICR estimation is able to converge rapidly, but not in a smooth manner. In Test 3, by introducing terrain vision, the ICR estimation can track the truths rapidly when terrain changes,

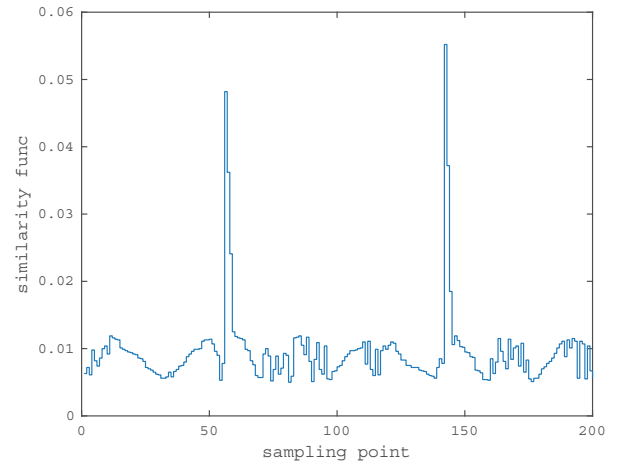


Fig. 4: Outputs of similarity function.

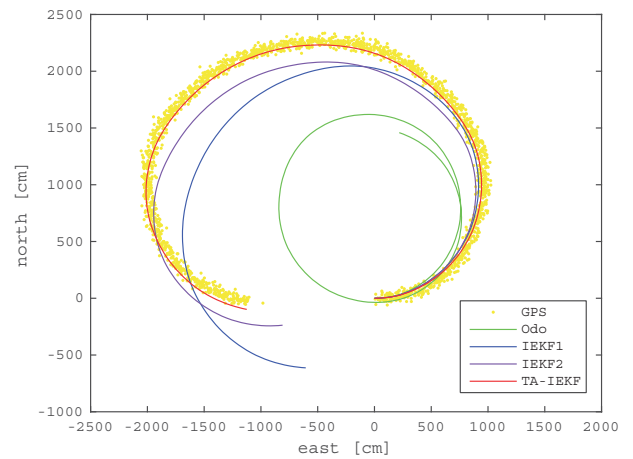


Fig. 5: Test results of dead reckoning based localization.

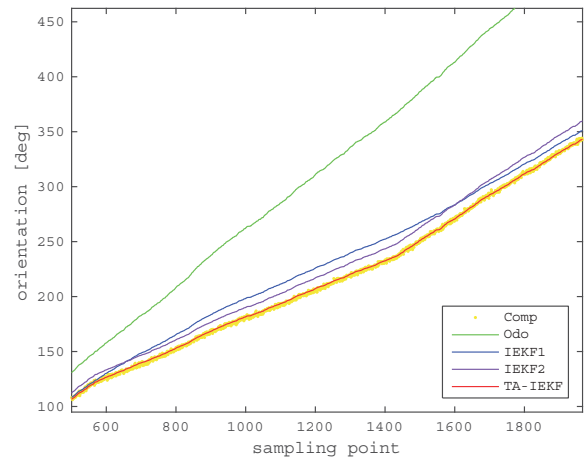


Fig. 6: Test results of dead reckoning based heading determination.

as shown in Fig. 3c. After the estimation being stable, it does not oscillate around the truths as that shown in Fig. 3b. Fig. 4 shows the the outputs of similarity function. Observe that the similarity function outputs a relatively large value

when terrain changes, thus it can be used as the indication of terrain variation. In Fig. 5 and Fig. 6, GPS stands for the outputs of GPS, Comp for the outputs of compass, Odo for the traditional dead reckoning, IEKF1 for the ICR dead reckoning where  $\bar{Q} = Q_{\min}$ , IEKF2 for the ICR dead reckoning where  $\bar{Q} = Q_{\max}$ , and TA-IEKF for the ICR dead reckoning where ICRs are estimated by using terrain adaptive IEKF. Due to the presence of slippages, the accuracy of the traditional dead reckoning is unacceptable. By applying the proposed terrain adaptive IEKF, the ICRs can be estimated with high accuracy, and therefore, the ICR dead reckoning has the highest accuracy. Although it is observed that the ICR dead reckoning diverge the outputs of GPS slightly at the destination, the divergence can be retarded to a great extent, which is of great significance to the localization in GPS-denied areas.

## V. CONCLUSIONS

In this paper, we proposed an on-line ICR estimation method by fusing incremental encoders, a compass and GPS. The data fusion unit is able to provide accurate global location, absolute heading and robot's ICRs in real time by using the proposed terrain adaptive IEKF. As shown in the real-world experiment conducted on a four-wheel mobile robot, the ICR estimation converges rapidly, yet maintains the smoothness. Additionally, with the aid of estimated ICRs, a terrain adaptive odometry can adjust the parameters of kinematics model automatically, and outperforms other methods which cannot acquire ICRs accurately and timely. In the future, we will consider other means to detect terrains, such as a vibration-based method which is not susceptible to illumination variation, to further improve the accuracy of ICR estimation.

## REFERENCES

- [1] R. Siegwart, I. R. Nourbakhsh, and D. Scaramuzza, *Introduction to autonomous mobile robots*. MIT press, 2011.
- [2] M. Reinstein, V. Kubelka, and K. Zimmermann, "Terrain adaptive odometry for mobile skid-steer robots," in *Proceedings of 2013 IEEE International Conference on Robotics and Automation*, pp. 4706–4711, IEEE, 2013.
- [3] J. Pentzer, S. Brennan, and K. Reichard, "The use of unicycle robot control strategies for skid-steer robots through the icr kinematic mapping," in *Proceedings of 2014 IEEE/RSJ International Conference on Intelligent Robots and Systems*, pp. 3201–3206, IEEE, 2014.
- [4] J. Pentzer, K. Reichard, and S. Brennan, "Energy-based path planning for skid-steer vehicles operating in areas with mixed surface types," in *Proceedings of 2016 American Control Conference*, pp. 2110–2115, IEEE, 2016.
- [5] J. Pentzer, S. Brennan, and K. Reichard, "On-line estimation of vehicle motion and power model parameters for skid-steer robot energy use prediction," in *Proceedings of 2014 American Control Conference*, pp. 2786–2791, IEEE, 2014.
- [6] T. M. Dar and R. G. Longoria, "Slip estimation for small-scale robotic tracked vehicles," in *Proceedings of 2010 IEEE American Control Conference*, pp. 6816–6821, IEEE, 2010.
- [7] W. Yu, O. Y. Chuy Jr, E. G. Collins Jr, and P. Hollis, "Analysis and experimental verification for dynamic modeling of a skid-steered wheeled vehicle," *IEEE Transactions on Robotics*, vol. 26, no. 2, pp. 340–353, 2010.
- [8] J. L. Martínez, A. Mandow, J. Morales, S. Pedraza, and A. García-Cerezo, "Approximating kinematics for tracked mobile robots," *The International Journal of Robotics Research*, vol. 24, no. 10, pp. 867–878, 2005.
- [9] Y. Wu, T. Wang, J. Liang, J. Chen, Q. Zhao, X. Yang, and C. Han, "Experimental kinematics modeling estimation for wheeled skid-steering mobile robots," in *Proceedings of 2013 IEEE International Conference on Robotics and Biomimetics*, pp. 268–273, IEEE, 2013.
- [10] J. Pentzer, S. Brennan, and K. Reichard, "Model-based prediction of skid-steer robot kinematics using online estimation of track instantaneous centers of rotation," *Journal of Field Robotics*, vol. 31, no. 3, pp. 455–476, 2014.
- [11] Y. Yao, K. Cheng, Z.-J. Zhou, B.-C. Zhang, C. Dong, and S. Zheng, "A novel method for estimating the track-soil parameters based on kalman and improved strong tracking filters," *ISA Transactions*, vol. 59, pp. 450–456, 2015.
- [12] F. Jiancheng and Y. Sheng, "Study on innovation adaptive ekf for in-flight alignment of airborne pos," *IEEE Transactions on Instrumentation and Measurement*, vol. 60, no. 4, pp. 1378–1388, 2011.